Experimental Studies of Diffusion on Fractal Surfaces

Lois Anne Zook and Johna Leddy*

Department of Chemistry, University of Iowa, Iowa City, Iowa 52242

Received: July 7, 1998; In Final Form: October 10, 1998

Composites are formed by sorption of Nafion, an ion exchange polymer, onto inert substrates of two different microstructures: microcylinders (neutron track etched membranes) and microspheres. Flux of a neutral redox probe (hydroquinone) through the composites is measured voltammetrically. Data for the microsphere composites are presented for variation in volume fraction and bead radii. Flux is shown to increase as the ratio of surface area of the substrate to volume of Nafion increases. The enhancement is ascribed to a facile surface diffusion domain at the interface between the Nafion and the inert substrates. Enhancements are larger in the microcylinder composites. Images of the microsphere composites appear fractal. For the microsphere composites, the power law relating flux to a characteristic dimension (microsphere radius) has an exponent of 0.78. A similar analysis for the cylinders has an exponent of 1. The analysis also shows that the fundamental transport rates of surface and bulk diffusion are little different in the two composites. Thus, the difference in the flux characteristics of the two classes of composites is ascribed to the microstructure of the interface as opposed to a change in the basic flux properties. (A linear fit of the microsphere composite data is statistically comparable that of the fractal fit; however, the conductivity exponent of one for the linear fit does not capture the dimensionality of the microsphere/Nafion interface.) The smallest microspheres of radius 0.055 μm form agglomerates of radius 1.25 to 1.5 μm, while their flux characteristics are consistent with an effective radius of 0.24 μm.

1. Introduction

In composite materials, the structure of the interface between the components of the matrix can impact transport through the composites, and surface diffusion processes can dominate transport processes in the matrix. In this paper, a comparison of hydroquinone flux through composites with two different microstructures is provided. One microstructure is microcylinders (neutron track etched membranes) and the other is microspheres. In each case, an ion exchange polymer, Nafion, is the second component in the matrix. Scanning electron micrographs of the microsphere composites appear fractal, and the flux data for these composites are fit by a fractal model with a conductivity exponent of 0.78. The flux data for the cylindrical composites are fit by a linear model. The microstructure is shown to play a pivotal role in determining the flux characteristics of the composite, while the basic transport processes of surface and bulk diffusion are little changed.

Previous studies have shown that flux through Nafion can be enhanced by casting Nafion into the cylindrical pores of neutron track etched polycarbonate membranes.[1−5] Nafion restructures along the walls of the cylindrical pores, providing zones of facile surface diffusion along the interface between the Nafion and the pore walls.[1,2] As the surface area of the pore wall increases with respect to the amount of bulk Nafion in the pore, the flux of the neutral redox probe, hydroquinone, through the pore increases.

In this study, a second high surface area support matrix, polystyrene microspheres, was examined. The transport of a redox probe, hydroquinone, was examined by rotating disk voltammetry. Flux through these composites also increased as the surface area of the support matrix increased relative to the volume of Nafion. The observed flux enhancement was less than that for the cylindrical composites. Micrographs revealed fractal structures were formed in the microsphere composites. Fractility implies a power law relationship between a measured property (e.g., flux) and a characteristic dimension (e.g., microsphere radius). The power law relationship between the flux and microsphere radius yielded a noninteger exponent of 0.78. The comparable value for the microcylinder composites was 1. This difference in the exponents reflects the difference in the efficiency of the transport path along the interface.

The analysis also showed that while the structure of the interface had a large impact on the efficiency of the transport process, the transport coefficients for the interface and the bulk were little altered by the microstructure.

2. Experimental Section

Composite Formation. Composites were made by micropipeting appropriate volumes of a 5% (w/v) suspension of Nafion in water and lower aliphatic alcohols (Aldrich) and a 2.5% (w/v) suspension of polystyrene microspheres in water (Polyscience) onto the electrode. After air drying the cocast films, the composites were dried in a vacuum desiccator for 1 h to remove any remaining solvents. Bead radii of 0.055, 0.11, 0.185, 0.245, and 0.54 μm were used, with the beads occupying from 9 to 63% of the composite volume. Simple Nafion films were similarly prepared, absent the microspheres. Composites were approximately 10 μm thick. Thickness and volume percent were calculated from the weight percent of the casting solutions, volumes pipetted, electrode area, and polymer densities. The polystyrene microspheres are reported by the manufacturer to have a density of 1.05 g/cm^3. The density of Nafion films cold

* Author to whom correspondence should be addressed. E-mail: johnaleddy@uiowa.edu. Phone: 319-335-1720. FAX: 319-335-1270.

10.1021/jp982883a CCC: $15.00
Published on Web 11/13/1998

cast from commercial suspension has recently been determined[6] to be 1.40 g/cm^3.

Electrochemical Measurements. The redox solutions of 2 mM hydroquinone 99%+ (Sigma) and 0.1 M nitric acid were made using high purity (18 MΩ) water (Milli-Q). Hydroquinone diffuses through the solution and composite to the electrode surface where it undergoes a two electron two proton oxidation to form benzoquinone. At this pH, both reactant and product are neutral. The electrochemical cell consisted of a Teflon sheathed glassy carbon working electrode (area of 0.44 cm^2), a platinum mesh counter electrode, and a silver wire quasireference electrode.

The glassy carbon working electrode was polished successively with 1.0, 0.1, and 0.05 μm silica particles on a Sevlt polishing cloth (Buehler). The electrode was rinsed with water and concentrated nitric acid and was sonicated in water for 7 min. Films were casted on the electrode as described above and then allowed to equilibrate in the redox solution for several hours before measurements were taken. In 0.1 M acid, hydroquinone is fully protonated and undergoes a two electron oxidation at appropriate potentials. Rotating disk measurements were made with an EG&G model 371 Potentiostat-Galvanostat, EG&G model 175 Universal Programmer, Pine Instruments ASR rotator, and Soltec X-Y recorder (VP-6424S). Rotation rates between 100 and 1600 rpm were used. Hydroquinone was electrolyzed through the film at an oxidative potential for 15 min before steady-state rotating disk currents were recorded. It had been previously determined that this was sufficient time for the system to achieve steady state.

The measured steady state current i_{meas} is also a measure of the steady state flux through the Nafion portion of the composite, $J_{meas} = i_{meas}/nFA\epsilon$ where n, F, A, and ϵ are, respectively, number of electrons transferred, Faraday's constant, electrode area, and porosity of the composite taken as the volume fraction of Nafion.[1] J_{meas} is restricted to flux through the Nafion portion of the composite because the microspheres are impermeable. For electrolysis under mass transport limited conditions, the measured flux is limited by the flux carried in the film or composite J_{comp} and the flux carried in this solution J_{soln} as by two resistances in parallel.

$$J_{meas}^{-1} = J_{comp}^{-1} + J_{soln}^{-1} \quad (1)$$

From the Levich equation,[7] $J_{soln} = 0.62c^*D_s^{2/3}\nu^{-1/6}\omega^{1/2}$, where, in the solution, c^* is the concentration of the redox probe (moles/cm^3), D_s is the diffusion coefficient of the redox probe, ν is the kinematic viscosity, and ω is the angular frequency of rotation (radians/s). Then, provided the microstructural features of the composite are at least 5-fold smaller than the hydrodynamic boundary layer ($\delta_0 = 1.61D_s^{1/3}\nu^{1/6}\omega^{-1/2}$; here, $\delta_0 > 48$ μm),

$$J_{comp} = \frac{c^*\kappa m}{l} \quad (2)$$

where l is the thickness of the film (cm). The effective extraction parameter and effective mass transport coefficient are κ and m (cm^2/s), respectively. κ is the ratio of concentration of redox probe in the Nafion portion of the composite to that in solution at equilibrium. In the absence of other transport phenomena, m is the diffusion coefficient.

For several rotation rates, a plot of J_{meas}^{-1} versus $\omega^{-1/2}$ yields a slope characteristic of transport in the solution and the intercept J_{comp}^{-1}. For hydroquinone, $D_s = 9.4 \times 10^{-6}$ cm^2/s.[2] Because c^* and l are known, the parameter κm is determined. Throughout the paper, κm is used to characterize flux through the composites. For each combination of microsphere radius and volume fraction of microspheres, at least three replicates were performed. The listed uncertainties are the standard deviations of these replicates.

Images. Composites were cast on silicon wafers and imaged by scanning electron microscopy (SEM). Micrographs were taken on a Hitachi S-2700 and a Hitachi S-4000 SEM. Magnification factors of 20× and 100× the microsphere radius were examined.

Titration. In previous studies,[2] the sulfonic acid groups of the Nafion were found to adsorb at monolayer coverage over the surface of polycarbonate neutron track etched membranes. This was determined by titration of the exchangeable sulfonate sites, as the sulfonates adsorbed on the surface were not available for exchange. Similar titrations were performed on Nafion films and Nafion/microsphere composites formed with 0.76 μm radius spheres and a ratio of microsphere surface area to Nafion volume (SA/vol) of 4.4×10^5 cm^{-1}. Free-standing films were prepared by casting polymer solutions into weighing boats, and then peeling out intact films after drying. Films were weighed and then soaked in concentrated nitric acid for 1 h to fully protonate the sulfonic acid exchange sites. The protonated films were rinsed in copious amount of deionized (Milli-Q) water and placed in 25 mL of 0.3 M sodium chloride for 1 h to allow the Na^+ to ion exchange with the H^+. The resulting solution was titrated with a potassium hydrogen phthalate standardized sodium hydroxide solution to the phenolphthalein endpoint. Experiments were performed in triplicate. The Nafion film had an equivalent weight of 1150 g/mol, in good agreement with the value of 1100 reported by the manufacturer. For the composite, 24% of the sulfonate sites were unavailable for exchange. This corresponds to a radius of 0.26 nm for each inactive sulfonate group, consistent with roughly monolayer coverage of inactive sulfonates over the surface of the microspheres. The value of 0.26 nm is twice that found previously for sulfonates adsorbed on the cylindrical pore walls of neutron track etched membranes.[2]

3. Results and Discussion

The methodology and basic transport model for the microsphere composites evolved out of a prior study of composites of Nafion inside the microcylinders of neutron track etched polycarbonate membranes. These cylindrical composites serve as a point of comparison for the fractal microsphere composites.

3.1. Cylinder Composites. Previously, we studied transport through composites formed by sorbing Nafion into the cylindrical pores of neutron track etched polycarbonate membranes.[1,2] Flux through the Nafion filled cylindrical pores was shown to increase with the ratio of surface area of the pore to the volume of Nafion. The data were modeled by a two component transport system in which facile flux was provided along the interface between the Nafion and pore wall, and bulk Nafion filled the remainder of the pore where flux was shown to be the same as that through a simple Nafion film. Because the sulfonate sites of the Nafion bind at monolayer coverage along the surface of the pore walls, the thickness of the interfacial zone δ was taken as the length of the side chain connecting the sulfonate groups to the Nafion fluorocarbon backbone, 1.5 nm.

Flux is measured through a cross sectional area. To equate the measured flux $\tilde{J}_{meas}$ to the flux along the wall $\tilde{J}_{wall}$ and the flux through the bulk Nafion in the remainder of the pore $\tilde{J}_{bulk}$ it is necessary to correct for the associated cross sectional areas. (Tildes indicate parameters for cylindrical geometry.)

$$\tilde{A}_{open}\tilde{J}_{meas} = \tilde{J}_{bulk}\tilde{A}_{bulk} + \tilde{J}_{wall}\tilde{A}_{wall} \quad (3)$$

For a cylinder, $\tilde{A}_{open}$ is the cross sectional area of a cylinder of radius R; $\tilde{A}_{open} = \pi R^2$. This area is subdivided into an outer shell, $\tilde{A}_{wall}$, and a central core, $\tilde{A}_{bulk}$, such that $\tilde{A}_{open} = \tilde{A}_{wall} + \tilde{A}_{bulk}$. The shell has a thickness, δ, such that $\tilde{A}_{wall} = \pi[R^2 - (R - \delta)^2] \cong 2\pi R\delta$ for $\delta \ll R$.

Normalizing eq 3 by $\tilde{A}_{open}$ and each flux by l/c^* yields

$$\widetilde{\kappa m}_{meas} = \widetilde{\kappa m}_{bulk}\frac{\tilde{A}_{bulk}}{\tilde{A}_{open}} + \widetilde{\kappa m}_{wall}\frac{\tilde{A}_{wall}}{\tilde{A}_{open}} \quad (4)$$

As $\tilde{A}_{bulk}/\tilde{A}_{open} = 1 - \tilde{A}_{wall}/\tilde{A}_{open}$ and $\tilde{A}_{wall}/\tilde{A}_{open} = 2\delta/R$

$$\widetilde{\kappa m}_{meas} = \widetilde{\kappa m}_{bulk} + [\widetilde{\kappa m}_{wall} - \widetilde{\kappa m}_{bulk}]\frac{2\delta}{R} \quad (5)$$

For hydroquinone, a plot of $\widetilde{\kappa m}_{meas}$ versus R^{-1} for $0.015 \le R \le 0.3$ μm yields $\widetilde{\kappa m}_{wall} = (7.0 \pm 0.3) \times 10^{-5}$ cm^2/s and $\widetilde{\kappa m}_{bulk} = (6 \pm 3) \times 10^{-7}$ cm^2/s. The value of $\widetilde{\kappa m}_{bulk}$ compares well to the value of κm determined for simple Nafion films of $(3.5 \pm 0.2) \times 10^{-7}$ cm^2/s.

3.2. Images and Fractility. In the current study, composites were formed of Nafion and polystyrene microbeads. For four microsphere radii and a volume fraction of microspheres of 0.5, scanning electron micrographs were recorded. In these micrographs, the magnification was set such that the micron bar is a fixed multiple of the bead radius. In Figure 1a−d, micrographs are shown where the micron bar is 100× the microsphere radius; in Figure 1e−h, the multiple is 20× the radius. The radii in the images are 0.54 μm (a and e), 0.185 μm (b and f), 0.11 μm (c and g), and 0.055 μm (d and h). Two aspects of these images are immediately apparent.

The images for the smallest microsphere (0.055 μm) differ from the images for the other radii in that these sphere cluster to form larger spheres, approximately 1 to 1.25 μm in radius.

For radii $\ge$ 0.11 μm, the images appear self-similar, independent of radii. Thus, images in Figure 1a−c resemble sculptured carpet samples, and images in Figure 1e−g resemble grapes. The self-similarity is sufficient that without labeling the images, it would not be possible to sort the images by microsphere radii based on visual information alone.

Self-similarity on different length scales is a visual characteristic of fractal structures. The mathematical expression of fractility is a power law relationship between a measured quantity, Y, and a characteristic length of the system, X, such that

$$Y = \alpha X^{-\mu} \quad (6)$$

where α is a constant and μ is the conductivity exponent. Mathematically, μ takes on different values depending on the symmetry of the system. Experimentally, μ can be measured if the characteristic length, X, is varied appropriately. It is a further characteristic of real (natural or random) fractal systems that the power law is applicable over a finite range of X.[8]

3.3. Microbead Composites of One Sphere Size. Microsphere composites were made in several formulations. The microsphere radius r was held constant, and the volume fraction of beads in the composite a was varied; alternatively, r was varied while a was held constant at 0.46.

3.3.1. Single Sphere Radius Composites. Results for composites of a single radius microsphere are summarized in Table 1. For a given microsphere radius, κm increases with a. Similarly, for a fixed microsphere volume fraction ($a = 0.46$ or 0.48), κm increases with decreasing r, with the exception of the $r = 0.055$ μm microspheres. The anomalous behavior of the smallest microspheres is consistent with their distinct SEM images. The points for the fixed volume fraction are boldfaced in the table. κm also increases with the ratio of the surface area of the microsphere to the volume of the Nafion (SA/vol).

Functional Dependence of κm on r and a. The fractal appearance of the micrographs suggests that the measured value κm may exhibit a power law dependence on r for $r \ge 0.11$ μm. The power law relationship of log κm to log r and log a is shown in Figure 2. On the left, for $a = 0.46$ for all radii except 0.185 μm where $a = 0.48$, a linear plot is shown for all points where $r \ge 0.11$ μm. The equation for this line, log $\kappa m = -(0.76 \pm 0.07)$ log $r - (9.5 \pm 0.3)$ with a correlation coefficient of 0.98, is consistent with a power law of $\kappa m \propto r^{-0.76}$. (If the regression is restricted to $a = 0.46$ and $r \ge 0.11$ μm, the slope is 0.781 ± 0.006 with a correlation of 0.99995.) Composites for the smallest radius sphere, shown as × in the figure, do not fall on the line, as expected based on the SEM images.

On the right side of Figure 2, data are plotted for composites formed with microspheres of $r = 0.185$ μm and varying a. The resulting regression line is log $\kappa m = (0.72 \pm 0.02)$ log $a - (5.72 \pm 0.02)$ with a correlation coefficient of 0.997. This suggests $\kappa m \propto a^{0.72}$.

These results suggest that a power law of the form $\kappa m \propto (r/a)^{-\mu}$ would fit the data. The surface area of the microspheres per unit volume (SA) is set by the number of microspheres per unit volume, $N_{sphere} = a(^4/_3\pi r^3)^{-1}$ and the surface area per sphere ($4\pi r^2$) or $SA = N_{sphere} \times 4\pi r^2 = 3a/r$. With the exception of the 0.055 μm radius sphere, all the data in Figure 2 coalesce to a single plot of κm versus log SA as shown in the center of Figure 2. The equation for this line is log $\kappa m = (0.78 \pm 0.05)$ log $SA - (4.4 \pm 0.1)$ with a correlation coefficient of 0.983. The data for the largest radius microspheres fall off this line as the relationship between κm and SA is somewhat more complicated, as addressed below.

3.3.2. Flux Expression for Microbead Composites. In Table 1, the ratios of surface area of the microspheres to volume of Nafion are reported as log(SA/vol). (The reported values for the smallest radius microspheres are based on the bead radius, not the cluster radius observed in the SEM images.) As with the cylinders, κm increases with SA/vol. Titration results indicate approximately monolayer coverage of sulfonates along the surface of the microspheres which establishes the unique interfacial domain of thickness δ. The two zone transport model is appropriate, and an equation analogous to eq 4 will apply for the microsphere composites.

To analyze all of the data for $r \ge 0.11$ μm, the term A_{wall}/A_{open} must be defined for the microspheres. Consider the geometry shown in Scheme 1.

For a composite of microspheres of radius r and volume fraction a, each sphere is embedded in a cubic volume b^3 such that $a = V_{sphere}/b^3 = {}^4/_3\pi r^3/b^3$. (This is only strictly true as long as $r \le b/2$ or $a \le {}^4/_3\pi(b/2)^3/(b)^3 = 4\pi/24 = 0.523$.) This yields $b = r(4\pi/3a)^{1/3}$. The cross sectional area for diffusion along the surface of the microspheres has a thickness δ such that at the equator of the microsphere where the angle above the equator θ is zero.

$$A_{wall}|_{\theta=0} = \pi[(r+\delta)^2 - r^2] = \pi(2r\delta + \delta^2) \quad (7)$$

$$\cong 2\pi r\delta \text{ for } \delta \ll r \quad (8)$$

However, the cross section will vary with the position θ above

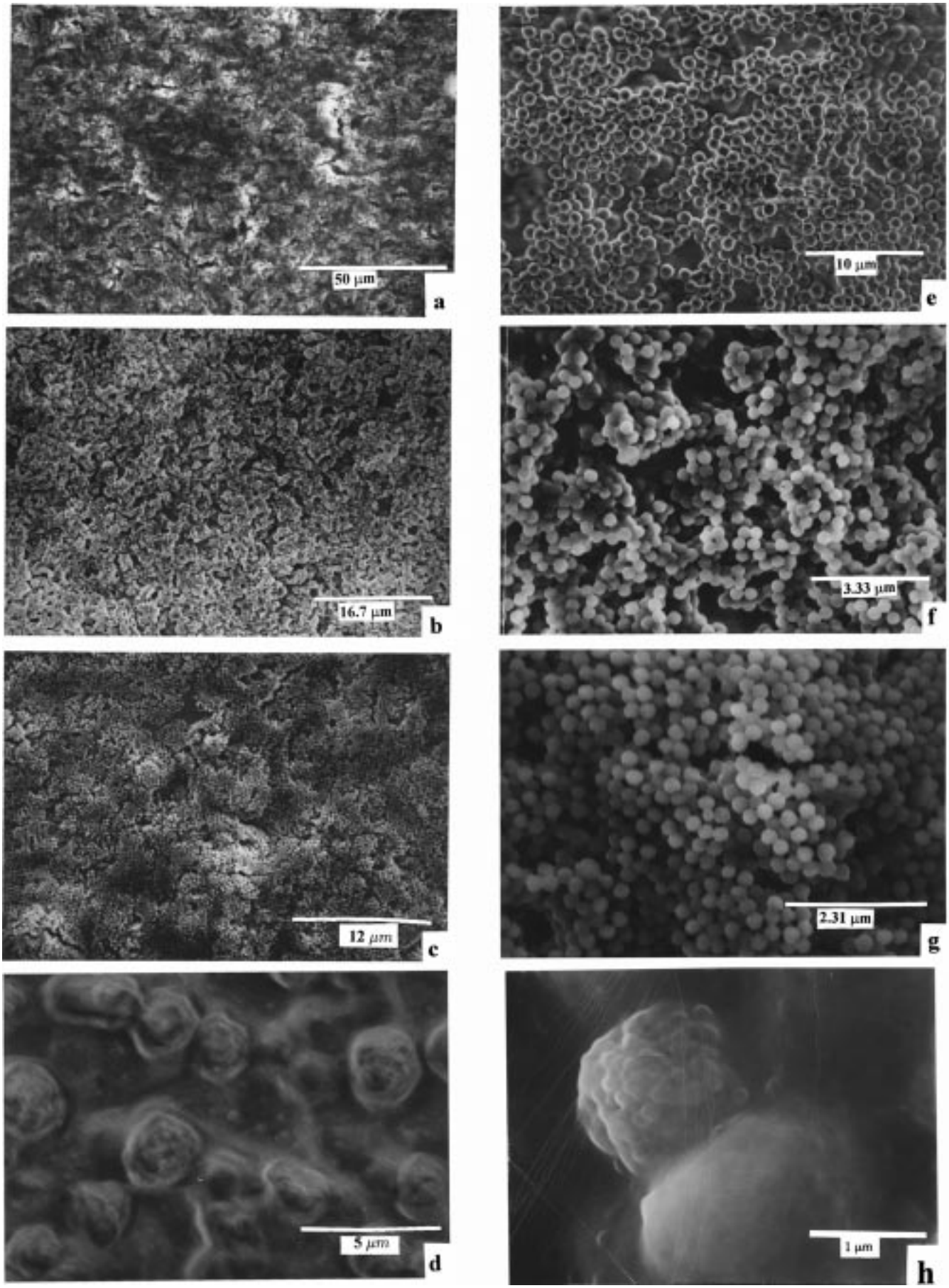

Figure 1. Scanning electron micrograph images of 50% by volume microspheres in Nafion. Images are taken so that, in each image, the micron bar is a fixed multiple of the microsphere radius. Images a−d are 100× the microsphere radius, and images e−h are 20×. Microsphere radii are 0.54 μm (a and e), 0.185 μm (b and f), 0.11 μm (c and g), and 0.055 μm (d and h).

TABLE 1: Data for Single Radius Microsphere Composites

r (μm)	a	κm (10^{-7} cm^2/s)	log (SA/vol) (cm^{-1})	A_{wall}/A_{open}
0.54	0.56	8.4 ± 1.3	4.85	0.00436
0.54	**0.46**	5.5 ± 0.8	4.68	0.00361
0.54	0.37	6.2 ± 0.1	4.51	0.00295
0.54	0.09	4.5 ± 0.6	3.74	0.00095
0.245	**0.46**	10.3 ± 0.4	5.02	0.00793
0.185	**0.48**	11.1 ± 1.2	5.18	0.01094
0.185	0.33	8.7 ± 2.8	4.90	0.00778
0.185	0.21	6.4 ± 1.2	4.63	0.00533
0.185	0.11	3.8 ± 0.2	4.30	0.00323
0.11	**0.46**	19.1 ± 2.1	5.37	0.01767
0.055	0.63	15.4 ± 3.8	5.97[a]	0.04821[a]
0.055	0.57	12.4 ± 0.8	5.86[a]	0.04352[a]
0.055	0.50	10.3 ± 2.4	5.74[a]	0.03826[a]
0.055	**0.46**	10.3 ± 2.4	5.67[a]	0.03533[a]
0.055	0.37	9.1 ± 0.3	5.50[a]	0.02860[a]
0.055	0.16	6.0 ± 0.1	5.02[a]	0.01446[a]
Nafion film		3.5 ± 0.2		

[a] SA/vol and A_{wall}/A_{open} calculated with $r = 0.055$ μm.

TABLE 2: Data for Microsphere Composites of Two Radii

r_1 (μm)	a_1	r_2	a_2	κm (10^{-7} cm^2/s)	log (SA/vol)[a] cm^{-1})
0.245	0.25	0.11	0.25	11.1 ± 0.8	5.30
0.245	0.167	0.11	0.333	13.3 ± 2.4	5.35
0.245	0.30	0.055	0.20	9.6 ± 1.7	5.46
0.11	0.375	0.055	0.125	16.6 ± 1.9	5.53
0.11	0.25	0.055	0.25	18.8 ± 3.7	5.61
0.11	0.125	0.055	0.375	15.7 ± 37.0	5.68

[a] SA/vol calculated with $r = 0.055$ μm.

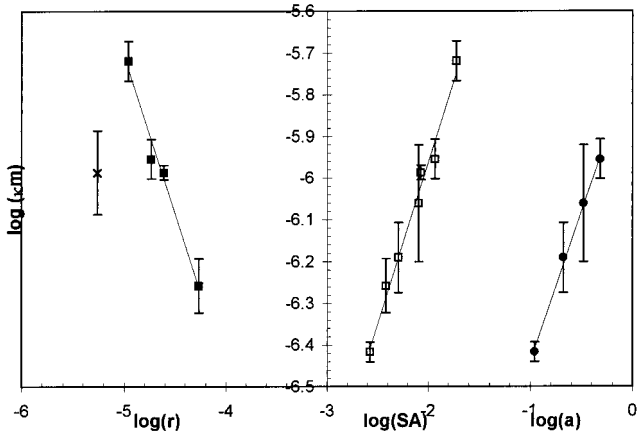

Figure 2. Plots to determine the conductivity exponent. On the left, log r κm is plotted versus log r for $a = 0.46$ for three bead radii, and $a = 0.48$ for r = 0.185 μm. (■). The point marked as × corresponses to $r = 0.055$ μm. On the right, log κm is plotted versus log a, for $r =$ 0.185 μm. (●). In the center, log κm versus log SA is plotted for all points except $r = 0.055$ μm, where SA = $3a/r$ (□).

the equator, such that the average area of the wall for the microspheres is

$$A_{wall} = \frac{2\pi\delta r\int_0^{\frac{\pi}{2}} \cos\theta \, d\theta}{\frac{\pi}{2}} \tag{9}$$

$$= 4\delta r \tag{10}$$

Similarly, the total cross sectional area occupied with Nafion at $\theta = 0$ is

$$A_{open}|_{\theta=0} = b^2 - \pi r^2 \tag{11}$$

SCHEME 1: Geometry for A_{wall}/A_{open}

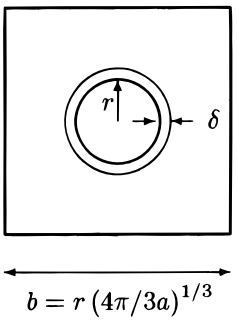

The variation in A_{open} with θ is restricted to the πr^2 term because the average radius is not descriptive of the relationship between b and r.

$$A_{open} = b^2 - \frac{\pi\int_0^{\frac{\pi}{2}}(r\cos\theta)^2 \, d\theta}{\frac{\pi}{2}} = b^2 - \frac{\pi}{2}r^2 \tag{12}$$

$$= r^2\left[\left(\frac{4\pi}{3a}\right)^{2/3} - \frac{\pi}{2}\right] \tag{13}$$

This yields A_{wall}/A_{open}

$$\frac{A_{wall}}{A_{open}} = \frac{4\delta}{r\left[\left(\frac{4\pi}{3a}\right)^{2/3} - \frac{\pi}{2}\right]} \tag{14}$$

The experimental data in Figure 2 suggest that the value of μ is between 0.72 and 0.78. A value of $\mu = 0.78$ is introduced into eq 4 to yield an expression for the microspheres.

$$\kappa m_{meas} = \kappa m_{bulk}\frac{A_{bulk}}{A_{open}} + \kappa m_{wall}\left[\frac{A_{wall}}{A_{open}}\right]^{0.78} \tag{15}$$

$$= \kappa m_{bulk}\left[1 - \frac{A_{wall}}{A_{open}}\right] + \kappa m_{wall}\left[\frac{A_{wall}}{A_{open}}\right]^{0.78} \tag{16}$$

The central portion of Figure 2 suggests the functional form of 15 should include a power dependence for a of $a^{0.78}$. However, the fit of log κm versus log SA did not incorporate the data for the largest radius microspheres. The expression based on A_{wall}/A_{open} incorporates all the data in Table 1 for $r \geq$ 0.11 μm and all but the two points where $A_{wall}/A_{open} \leq 0.0032$; a regression of log κm versus log A_{wall}/A_{open} indicates $\mu = 0.78$ ± 0.10. A development based on A_{wall}/A_{open} is formally correct as the flux expression is derived by normalization with A_{open}, as appropriate to the area dependency of flux.

The theoretically expected conductivity exponent for a finitely ramified structure[9] is defined by

$$\mu = \frac{\ln\left[\frac{d+3}{d+1}\right]}{\ln 2} + d - 2 \tag{17}$$

where d is the dimension of the surface. For the experimentally determined value of $\mu = 0.78$, $d = 2.05$. This agrees well with the dimensionality of two previously determined for the microspheres.[10,11] Deterministic fractal structures are generated through a recursion process, and exhibit fractal behavior over all characteristic dimensions. A Sierpinski gasket is an example. For a deterministic fractal such as a Sierpinski gasket where d

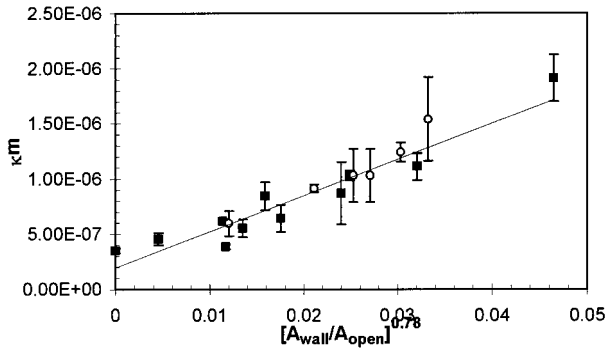

Figure 3. Plot of the microsphere composite data according to fractal model. Plot of κm with $(A_{wall}/A_{open})^{0.78}$ for $r \geq 0.11$ μm (■), and the smallest radius fit to the effective radius 0.24 μm (○).

$= 2$, eq 17 yields a value of μ of 0.737. The similarity to the experimentally determined value of 0.78 suggests that diffusion along the surface of the microspheres has some similarities to diffusion across a Sierpinski gasket.

3.3.3. Results for Composites: $r \geq 0.11$ μm. The results of a plot for the data in Table 1 where $r \geq 0.11$ μm based on eq 15 is shown in Figure 3. Regression of all the data including the Nafion film, of κm with (A_{wall}/A_{open}) yields $\kappa m_{wall} = (3.3 \pm 0.3) \times 10^{-5}$ cm^2/s and $\kappa m_{bulk} = (2.0 \pm 0.8) \times 10^{-7}$ cm^2/s with a correlation coefficient of 0.91. Note that the term $1 - A_{wall}/A_{open} \rightarrow 1$ for composites where $r \geq 0.11$ μm. For the microcylinder composites, the values found were $\widetilde{\kappa m}_{wall} = (7.0 \pm 0.3) \times 10^{-5}$ cm^2/s and $\widetilde{\kappa m}_{bulk} = (6 \pm 3) \times 10^{-7}$ cm^2/s. For the microsphere composites, κm_{wall} is approximately half that found for the microcylinder composites. The κm_{bulk} value is also about half of that found for a simple Nafion film, $(3.5 \pm 0.2) \times 10^{-7}$ cm^2/s. A factor of two difference for ion exchange polymer composites is not a large difference, but the difference is above the uncertainty in these results.

The highest value of κm is observed for $a = 0.46$ and $r = 0.11$ μm, where κm is 5.5-fold higher than that observed for a simple Nafion film. As expected for a facile surface transport mechanism, this sample has the highest ratio SA/vol at 2.34×10^5 cm^{-1}. The microcylinder composites yield a maximum κm value of 1.5×10^{-5} cm^2/s or a flux enhancement of about forty fold higher than a simple Nafion film. This is for SA/vol of about 3.8×10^5 cm^{-1}. Despite the similarity in the ratio of SA/vol for the two types of composites, the net flux through the Nafion filled portion of the composites, is significantly higher in the microcylinder composites. This highlights the importance of the interfacial structure in determining the net flux through the composites and is reflected in the power dependence of A_{wall}/A_{open} for the cylinders ($\mu = 1$) and spheres ($\mu = 0.78$). Further, the drastic difference in the flux enhancement is driven almost entirely by the difference in the two microstructures, as is apparent from the relatively similar values found for κm_{wall} and κm_{bulk} for the two types of composites.

In real fractal systems, the range of fractal behavior is bounded, so it may not be appropriate to apply the analyses over an infinite range of A_{wall}/A_{open}. However, restricting the regression to $A_{wall}/A_{open} > 0.0032$ had little impact; it yielded a 10% higher value of κm_{wall}, drove the intercept toward zero, and did little to improve the correlation.

Recently, the importance of the range over which fractal behavior is observed has been discussed.[12] In the composites studied here, the radii found to comply with a fractal model ranged from 0.11 to 0.54 μm or over about 0.7 of a decade in radius. The characteristic length used to fit the data was A_{wall}/A_{open} which ranged from 0.00098 to 0.0196 for $r \geq 0.11$ μm. This is a 20-fold change or about 1.3 decades. For these composites, the radius was limited by clustering of the microspheres for $r = 0.055$ μm and a measurable effect at lower surface areas (low a and large r). Similar limitations of packing and measurable effect also limited the flux enhancements observed in the cylindrical composites.

The data can also be analyzed using a simple linear model where the conductivity exponent of 0.78 in eq 15 is replaced with 1. This is analogous to the model used to analyze the microcylinder composites. Under these conditions, the data shown in Figure 3 are characterized by $\kappa m = (7.8 \pm 0.6) \times 10^{-5}$ $(A_{wall}/A_{open}) + (3.0 \pm 0.5) \times 10^{-7}$, with a correlation coefficient of 0.94.

The linear and fractal analyses yield values of κm_{bulk} ($(3.0 \pm 0.5) \times 10^{-7}$ and $(2.0 \pm 0.2) \times 10^{-7}$ cm^2/s,, respectively) that are in similar agreement with κm_{Nafion} for a simple Nafion film, ($(3.5 \pm 0.2) \times 10^{-7}$ cm^2/s). Such agreement is typical of composites formed by sorbing polymer onto polymer, because the variability of both the polymers and composite formation is higher than the variability of single component, bulk phases. Such variability is reflected in $\widetilde{\kappa m}_{bulk}$ of $(6 \pm 3) \times 10^{-7}$ cm^2/s. For the microsphere composites in Table 1, the relative standard deviations of the measured κm values is 13%; the relative standard deviations for the cylindrical composites are reported as less than 20%, with the exception of the 25 nm pores, where it is 33%. For the cylindrical composites, uncertainty in the porosity is also a factor. The uncertainties reported here for the slopes and intercepts only reflect the uncertainties in the regression, not the uncertainties associated with each datum. The values found for κm_{wall} for the linear ($(7.8 \pm 0.6) \times 10^{-5}$ cm^2/s) and fractal ($(3.3 \pm 0.3) \times 10^{-5}$ cm^2/s) analyses for the microsphere composites, agree within a factor of two. The linear analysis yields a value slightly closer to that of the cylindrical composites, $\widetilde{\kappa m}_{wall} = (7.0 \pm 0.3) \times 10^{-5}$ cm^2/s. However, given the large relative standard deviations of the measured κm values, and the general variability of the composites, the κm_{wall} values for the linear and fractal analyses are not remarkably different in the context of polymer composites.

The fractal analysis can be argued as more appropriate based on several observations. First, the log κm analysis of Figure 2 yields a value of μ between 0.72 and 0.78. Second, the dimensionality of microspheres has been found to be 2.0 [10,11]. The images in Figure 1 show a surface which is not smooth, but rather looks self similar on different length scales, consistent with a fractal surface. Third, the range of μ of 0.72−0.78 found in analyses of Figure 2 corresponds to dimensionality d between 1.98 and 2.06. Given the functional form of Equation 17, this number is very distinct from d of 2.32 found when $\mu = 1$. From the images, and the reported values of microsphere dimensionality, the fractal analysis is physical more consistent with what is known about the system.

3.3.4. Composites where $r = 0.055$ μm. SEM images for composites formed of a single bead radius where the radius was $r = 0.055$ μm had a different appearance than the composites formed with larger microspheres. These microspheres agglomerated into larger spherical structures where agglomerate means subunits adhere to make a mechanical robust larger unit.[13] The agglomerated structures had a radius of 1.25 to 1.5 μm from the SEM images.

For the cylindrical composites, unusual packing behavior was also observed for the smallest radius cylinders ($R = 0.075$ μm).[1] For this structure, it was shown geometrically that the 1.5 nm chains linking the sulfonate groups to the polymer backbone were too crowded to pack at the same density as was possible

in the larger pores. It is probable that the packing constraints on the smallest microspheres also result in similar crowding. While the cylindrical pores were rigid, during casting the microspheres can be moved in the casting solvents to form agglomerates and eliminate the strain associated with trying to pack the smallest spheres into the same extended structure exhibited by the larger microspheres.

Attempts to analyze the data for the smallest microsphere composites following the protocol for the larger microspheres were unsuccessful. However, in the left hand side of Figure 2, the point for the smallest microsphere ($\times$ on the plot) is shifted onto the line with the other composites where $a = 0.46$ if the real radius of 0.055 μm is replaced with 0.24 μm. When this radius is substituted for the 0.055 μm radius data in Table 1, all the smallest size bead data are brought into agreement with the larger radii data. This is illustrated in Figure 3 by the open circles. Regression of this line yields an expression statistically the same as that found for the larger microsphere composites ($\kappa m = (3.4 \pm 0.3) \times 10^{-5}\ A_{wall}/A_{open} + (1.8 \pm 0.6) \times 10^{-7}$ with a correlation coefficient of 0.91). This suggests that the factors dictating transport inside the agglomerated structures are similar to the factors operating in the extended structures.

The effective radii of 0.24 μm is larger than the actual radius of the beads (0.055 μm) but smaller than the radius of the agglomerated clusters shown in Figure 1d and h (1.25 to 1.5 μm). The effective radius encapsulates about twenty microspheres and the agglomerate encapsulates about 500 microspheres. The effective size of a cluster can differ from the perimeter measured for a cluster because of encapsulated holes in the structure; the holes contribute to the surface area.[14] In the present case, this corresponds to a higher effective surface area (smaller effective radius) than is measured for the agglomerate radius by SEM.

3.4. Microbead Composites of Mixed Sphere Sizes Composites. Composites were formed by mixing together microspheres of two different sizes. The results are summarized in Table 2. No attempt was made to determine A_{wall}/A_{open} for these composites. However, SA/vol is easily calculated by summing the surface area generated by each microsphere size and then dividing by the total volume of Nafion. From Table 2, κm increases with SA/vol for composites containing 0.055 μm radius microspheres. Facile surface diffusion contributes to the net flux through these composites as well. Clustering in these composites was not well characterized, and no attempt has been made to correct for clustering effects.

4. Summary

These composites provide a rich variety of characteristics, as well as some design paradigms for microstructured materials. (1) Microsphere and microcylinder composites enhance flux as the surface area of the microstructured support increases relative to the volume of the ion exchange polymer, Nafion. This is ascribed to a facile surface diffusion process. (2) SEM images of microsphere composites appear fractal. (3) Flux enhancement is more dramatic in microcylinder composites than in microsphere composites. Analysis based on the fractility of the interface between the Nafion and the surface of the microstructured support indicates that the basic transport processes of surface and bulk transport are not drastically affected by the microstructure. (4) The power law relationship between the flux and the characteristic dimension of the microstructured support yields exponents of 0.78 for the microspheres and 1.0 for the cylinders. This dependence dominates the net flux through the composites, and the straight path of the cylinder is more effective at enhancing flux than the more tortuous path of the microspheres. The noninteger conductivity exponent of the microsphere composites is consistent with the fractal appearance of the SEM images. (5) The smallest microspheres ($r = 0.055$ μm) agglomerate to form larger clusters ($r_{clusters} =$ 1.25 to 1.5 μm). The flux data for these composites are brought into registry with the data for the larger composites by using an effective radius of 0.24 μm. This is consistent with similar basic transport processes occurring within the agglomerates and the agglomerates having larger internal surface area than is measured by the radius of the agglomerate in the SEM image. (6) For microstructured materials, flux can be enhanced by increased internal surface area. The nature of the microstructure itself has greater impact on the net flux through the composite than changes in the basic transport processes.

Acknowledgment. The financial assistance of the National Science Foundation (Grant CHE-93-20611) is gratefully acknowledged. Discussions with Alex Scheeline of the University of Illinois are appreciated.

References and Notes

(1) Fang, Y.; Leddy, J. *J. Phys. Chem.* **1995**, *99*, 6064−6073.
(2) Leddy, J.; Vanderborgh, N. E. *J. Electroanal. Chem.* **1987**, *235*, 299−315.
(3) Penner, R. M.; Martin, C. R. *J. Electrochem. Soc.* **1985**, *132*, 514−515.
(4) Liu, C.; Martin, C. R. *J. Electrochem. Soc.* **1990**, *137*, 510−515.
(5) Liu, C.; Martin, C. R. *J. Electrochem. Soc.* **1990**, *137*, 3114−3120.
(6) Zook, L. A.; Leddy, J. *Anal. Chem.* **1996**, *68*, 3793−3796.
(7) Bard, A. J.; Faulkner, L. R. *Electrochemical Methods*; John Wiley & Sons, Inc.: New York, 1980; p 288.
(8) Harrison, A. *Oxford Chemistry Primers*; Oxford University Press: New York, 1995; Vol. 22 (*Fractals in Chemistry*).
(9) Havlin, S. In *The Fractal Approach to Heterogeneous Chemistry*; Avnir, D., Ed.; John Wiley & Sons, Inc.: New York, 1989; pp 249−257.
(10) Pusey, P. N.; Rarity, J. G. *Mol. Phys.* **1987**, *62*, 411−418.
(11) Zhou, Z.; Chu, B. *J. Colloid Interface Sci.* **1991**, *143*, 356−365.
(12) Ofer, M.; Lidar, D. A.; Biham, O.; Avnir, D. *Phys. Rev. E* **1997**, *56*, 2817−2828.
(13) Kaye, B. H. *A Random Walk through Fractal Dimensions*; VCH Publishers: New York, 1989; p 14.
(14) Stauffer, D. *Introduction to Percolation Theory*; Taylor and Francis, Ltd.: Philadelphia, 1985; p 59.